Multilayered crystals of macroions under slit confinement

2009 J. Phys.: Condens. Matter 21 424110

(http://iopscience.iop.org/0953-8984/21/42/424110)

J. Phys.: Condens. Matter **21** (2009) 424110 (8pp) doi:10.1088/0953-8984/21/42/424110

Multilayered crystals of macroions under slit confinement

E C Oğuz, R Messina and H Löwen

Institut für Theoretische Physik II: Weiche Materie, Heinrich-Heine-Universität Düsseldorf, Universitätsstraße 1, D-40225 Düsseldorf, Germany

E-mail: ecoguz@thphy.uni-duesseldorf.de, messina@thphy.uni-duesseldorf.de and hlowen@thphy.uni-duesseldorf.de

Received 20 April 2009
Published 29 September 2009
Online at stacks.iop.org/JPhysCM/21/424110

Abstract

The crystalline ground state of macroions confined between two neutral parallel plates in the presence of their homogeneously spread counterions is calculated by lattice sum minimization of candidate phases involving up to six layers. For increasing macroion density, a cascade of solid–solid transitions is found involving various multilayered crystals. The cascade includes triangular monolayer and buckled bilayer as well as rhombic, squared and triangular phase structures.

(Some figures in this article are in colour only in the electronic version)

1. Introduction

Strong correlations in Coulomb systems lead to a variety of new effects which are absent for neutral particles, see, e.g., [1, 2] for a review. Among those are nonlinear screening effects [3–6], charge inversion [7], Coulomb criticality [8, 9], like-charge attraction for multivalent ions [10–13] as well as exotic binary crystalline structures unknown for uncharged systems [14, 15].

By using charged colloidal suspensions [16] or dust particles in plasmas [17], it is possible to realize strongly asymmetric mixtures of oppositely charged particles. These systems consist of mesoscopic highly charged 'macroions' and microscopic counterions with a low valence, resulting in strong charge and size asymmetries. Since the charges of the macroions are high, strong Coulomb correlations are typical for macroions. Most of the physics can still be captured by viewing these systems as strongly asymmetric and strongly coupled electrolytes. In recent years, it was possible to confine macroions in sheets between two parallel plates [18, 19, 16, 20, 21] and to observe the resulting lateral structure of the particles. The gross features can be understood in terms of an (effective) one-component system with a Yukawa pair interaction [22–27]. In fact, the mono and bilayer ground-state structures which were obtained from a Yukawa model [28] describe the experimentally found structures [29]. For multilayers beyond the bilayer regime, a rich variety of stable phases are found in experiments [30–32] as well as in simulations [33], which are all theoretically confirmed for a Yukawa system between two neutral walls [34]. This motivates a study about the influence of the wall–particle interaction on the phase behavior of multilayered crystalline sheets in slit-like confinement [35].

In this paper, we consider a model for macroions confined between two parallel neutral walls[1]. There is a direct Coulomb interaction between the point-like particles. The total system is charge-neutral and the counterions are kept at high temperature and are homogeneously spread between the plates, resulting in an attraction acting on the macroions towards the middle of the plates. The system is realized for highly charged colloidal particles or dust particles in plasmas. Some early theoretical and simulational investigations on clusters of artificial atoms [37–39] and dusty plasmas [40, 17] as well as one-component plasmas [41–43], including all the parabolic potentials acting as confinement, reveals the existence of multilayers. We therefore include the regime beyond bilayers in our discussion. Lattice sum minimizations among a broad set of candidate structures are used to determine the structure which minimizes the potential energy per particle. For increasing macroion density, we find a cascade of solid–solid transitions which includes triangular monolayer, buckled bilayer and squared, rhombic and triangular bi, tri, tetra, penta and hexalayers[2]. Comparing the results to those

[1] Different from [36] we include here a neutralizing background of counterions.

[2] For colloid–polymer films, see [44].

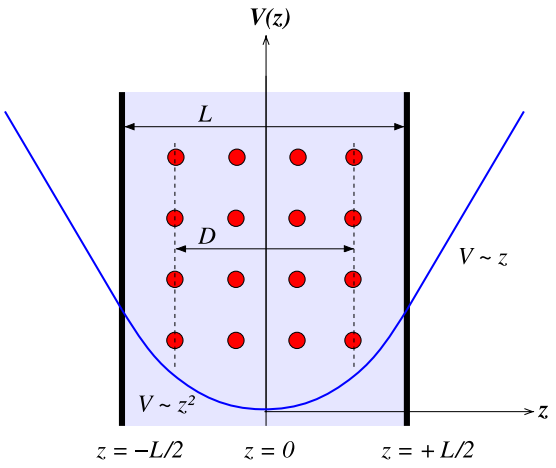

Figure 1. A schematic illustration of the model. The ions (e.g. charged colloids) are represented by filled circles. The counterions are smeared out between the two hard walls located at $z = \pm L/2$. This charge distribution generates a quadratic potential $V(z) \sim z^2$ in between as shown. The separation between outermost layers (dashed lines) is denoted by D.

involving a Yukawa interaction [34], we show that the topology of the phase diagram depends crucially on the particle–wall interaction. In fact, some complicated tetralayered structures which were found stable for the confined Yukawa model are unstable in the present model. The strong correlation between phase behavior and wall–particle interactions suggests tailoring new crystalline structures (e.g. with desired filtering properties [45]) by a suitable surface treatment of the plates.

This paper is organized as follows. The model is introduced in section 2. After discussing the structure of different crystalline multilayers, results for the cascade of solid–solid transitions are presented in section 3. Finally we conclude in section 4.

2. The model

We consider N classical point-like particles of charge q (*macroions*) interacting via the unscreened Coulomb pair potential

$$V(r) = \frac{q^2}{\epsilon r}, \tag{1}$$

where r denotes the interparticle distance and ϵ the (relative) dielectric constant of the surrounding medium. The system is confined between two parallel hard walls of area A and separation L, see figure 1. The global charge neutrality of the system is ensured by counterions. The latter are taken into account by a homogeneous neutralizing background that is smeared out over the whole slit. We mention that we neglect the discrete nature of the counterions in this approach, as well as any local ion–counterion coupling.

As a consequence of the Gauss law, the electric field E_b (stemming from the neutralizing background) is linear in z inside the slit and constant outside the slit. More specifically, we have

$$E_\mathrm{b}(z) = \begin{cases} -\dfrac{4\pi}{\epsilon}\dfrac{Nq}{A}\dfrac{z}{L} & \text{for } -L/2 \leqslant z \leqslant +L/2, \\ -\dfrac{2\pi}{\epsilon}\dfrac{Nq}{A}\dfrac{z}{|z|} & \text{else.} \end{cases} \tag{2}$$

We thereby implicitly neglect image charge effects [46], meaning that we assume there is no dielectric contrast at the interfaces (at $z = \pm L/2$). The resulting electrostatic potential Φ_b, verifying the matching condition at $z = \pm L/2$, then is

$$\Phi_\mathrm{b}(z) = \begin{cases} \dfrac{2\pi\eta q}{\epsilon L^3} z^2 & \text{for } -L/2 \leqslant z \leqslant +L/2, \\ \dfrac{2\pi\eta q}{\epsilon L^2}|z| - \dfrac{\pi\eta q}{2\epsilon L} & \text{else,} \end{cases} \tag{3}$$

where the reduced density

$$\eta \equiv \frac{N}{A} L^2 \tag{4}$$

was introduced. Hence, the potential of interaction $V_\mathrm{b}(r)$ between a macroion and the counterion background is merely given by

$$V_\mathrm{b}(z) = q\,\Phi_\mathrm{b}(z). \tag{5}$$

We are now in a position to write the total potential energy per particle u as[3]

$$u = \frac{1}{2N}\sum_{i=1}^{N}\sum_{j=1}^{N} V(r_{ij}) + \frac{1}{N}\sum_{i=1}^{N} V_\mathrm{b}(z_i). \tag{6}$$

In its appropriate rescaled form, u is (within the slit)

$$u\frac{\epsilon L}{q^2} = \frac{1}{2N}\sum_{i=1}^{N}\sum_{j=1}^{N}\frac{1}{r_{ij}^*} + \frac{1}{N}\sum_{i=1}^{N} 2\pi\eta z_i^{*2}, \tag{7}$$

with $r_{ij}^* \equiv r_{ij}/L$ and $z_i^* = z_i/L$, showing that at the prescribed confinement width L the energy of the system depends only on η. Consequently the phase diagram at zero temperature is given as a function of η.

At each given density η, we have performed lattice sum minimizations for a broad set of candidates of crystalline lattices. In order to handle the long ranged Coulomb potential, we have used the Lekner summation method [47] for three-dimensional systems with two-dimensional periodicity [48], see also [49]. More explicitly, we consider in this work three-dimensional crystals with two-dimensional periodicity in the x and y directions whose primitive cell is a parallelepiped containing n particles. This parallelepiped is spanned by the three lattice vectors $\mathbf{a} = a(1, 0, 0)$, $\mathbf{b} = a\gamma(\cos\theta, \sin\theta, 0)$ and $\mathbf{c} = D(0, 0, 1)$, where γ is the aspect ratio ($\gamma = |\mathbf{b}|/|\mathbf{a}| = b/a$) and θ is the angle between $\mathbf{a}$ and $\mathbf{b}$. Furthermore, the n particles are distributed, not necessarily evenly, on m

[3] To remedy the divergence occurring with the first term of (6), a *two-dimensional* neutralizing background is introduced in the Lekner (or equivalently Ewald) sum. This neutralizing background (implicitly present in the Lekner and/or Ewald sum) has to be distinguished from the one that we use to model the counterions, which is smeared out over the whole *volume* of the slit.

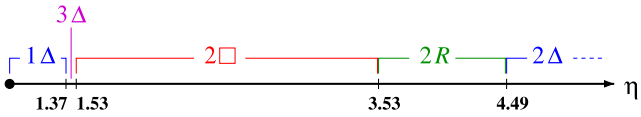

Figure 2. Stability phase diagram of crystalline mono and bilayers. The five stable phases 1Δ, 3Δ, 2□, 2R and 2Δ correspond to Wigner crystals, found in earlier investigations (see text for details). Note that the monolayer–trilayer transition occurs at $\eta \approx 1.37$.

layers in the z direction such that $c = |\mathbf{c}|$ corresponds to the distance between outermost layers (see also figure 1). Hereby we restrict ourselves to layered situations with an up–down inversion symmetry in the averaged occupancy reflecting the up–down symmetry of the confining slit. Under this sole restriction, we consider possible candidates with $n = 1, \ldots, 8$ and $m = 1, \ldots, 6$ up to symmetric six-layer structures with a basis of up to 8 particles. Furthermore, we also examine the stability of several asymmetric buckling phases, as predicted in [50]. For given η, the total potential energy per particle is minimized with respect to the particle coordinates of the basis and the cell geometry (γ and θ). The resulting stability phase diagrams are shown and discussed in the following sections.

3. Mono and bilayer phase behavior

3.1. Phase diagram

An increase of η within the mono and bilayer regime reveals the existence of five stable crystalline mono and bilayers: 1Δ (triangular), 3Δ (staggered triangular), 2□ (square), 2R (rhombic) and 2Δ (staggered triangular). The integers indicate the number of layers. For increasing η, the stability cascade therefore is

$$1\Delta \rightarrow 3\Delta \rightarrow 2\square \rightarrow 2R \rightarrow 2\Delta. \qquad (8)$$

Most of these phases, corresponding to Wigner crystals predicted in earlier theoretical investigations [36, 28], are also found in experiments on charged colloidal suspensions [51, 52] as well as in Monte Carlo simulations of confined hard spheres [53]. The detailed phase diagram is reported in figure 2.

We emphasize that the 3Δ phase (staggered in an ABC manner, see also table 1) intervenes between 1Δ and 2□ rather than a buckled phase which is present in a situation where the external potential has a vanishing curvature at the origin.

At small reduced densities η, particles tend to stay in the potential minimum (cf figure 1) created by the counterion background. This is precisely the origin of the stability of monolayered Wigner crystals, which never occurs in purely unscreened Coulomb systems[4]. The triangular monolayer 1Δ is stable up to $\eta = 1.37$. At larger densities the mutual repulsive interparticle interactions, the first term in equation (7), dominates the competition between

[4] Indeed, we found that a rectangular bilayer with size ratio $\gamma = \sqrt{3}$, proposed as a stable structure for very small η in [36], is always energetically beaten by a buckled (2B) bilayered phase. Seen from the top, this structure corresponds to the triangular lattice.

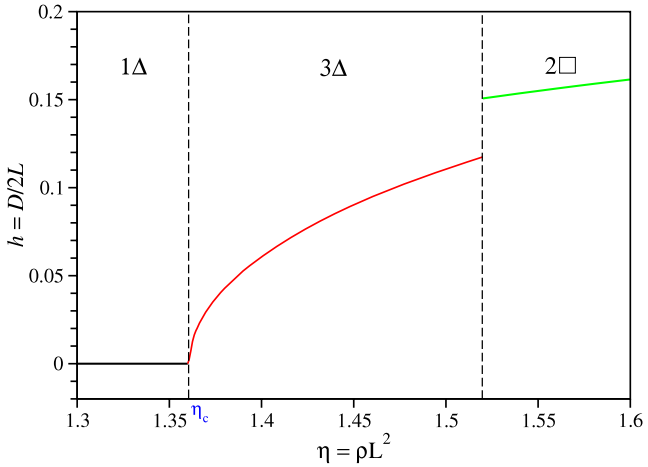

Figure 3. Order parameter h in the transition regime 1Δ to 2□ via 3Δ. The monolayer 1Δ buckles at a critical density $\eta_c \sim 1.360\,901$ to a trilayer.

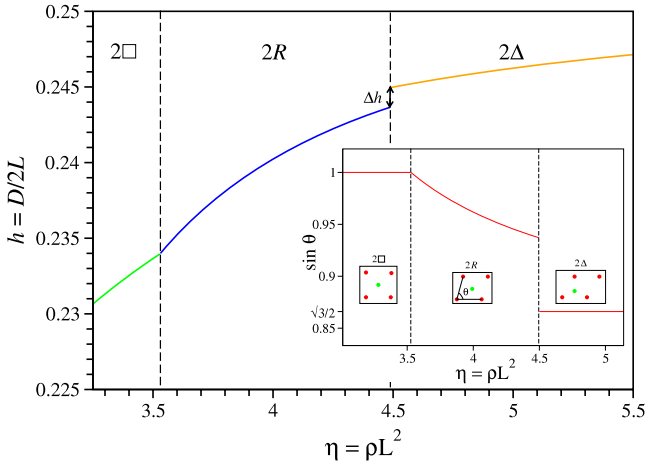

Figure 4. Order parameter h in the transition regime 2□ to 2Δ via 2R. The discontinuity Δh at the transition 2R → 2Δ is also shown for clarity. The profile of $\sin\theta$ (with its corresponding structures) is also shown as an inset. Thereby, the outer particles belong to a given layer whereas the inner particle belongs to the other one.

the interparticle (macroion–macroion) repulsion and particle–background (macroion–counterion) attraction.

The structure with triangular base shape 3Δ appears as the first stable multilayer (see figure 3) interpolating between 1Δ and 2□. The associated order parameter, namely the separation

$$h \equiv \frac{D}{2L} \qquad (9)$$

between the mid-plane and the outer macroion layer (see also figure 1), is continuous at the transition 1Δ → 3Δ but discontinuous across the 3Δ → 2□ transition, see figure 3 and [53].

By further increase of η, one recovers the rhombic phase 2R, which is continuously achievable from the square phase 2□ by changing θ, as indicated in the inset of figure 4. The two geometrical order parameters h and $\sin\theta$, see figure 4, indicate

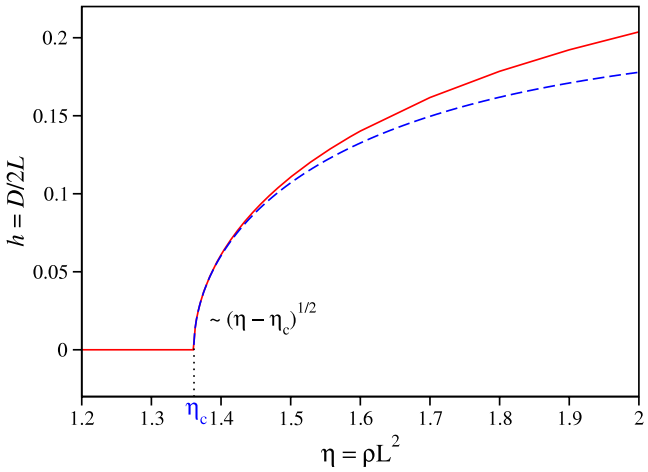

Figure 5. Plot of equation (14) (dashed line) and numerical calculations for finite $h(\eta)$ (solid line) based on full lattice sum minimization near the monolayer–trilayer $1\Delta \rightarrow 3\Delta$ transition.

thereby a continuous transition for $2B \rightarrow 2\square$. On the other hand, at larger values of η, the transition $2R \rightarrow 2\Delta$ is of first order as signaled by the jumps of the two geometrical order parameters h and $\sin\theta$, see figure 4. The staggered triangular phase 2Δ corresponds to the ultimate stable structure in the high density regime of bilayers.

3.2. From monolayer to trilayer—an analytic approach

We now would like to address the transition $1\Delta \rightarrow 3\Delta$ analytically. To do so, we apply a Taylor expansion to $u(h)$ around $h = D/2L = 0$, see the appendix for details. The resulting asymptotic expression for small interlayer distances h reads

$$\frac{u(h)}{q^2/\epsilon L} = B_0\sqrt{\eta} + B_1\eta^{3/2}h^2 + B_2\eta^{5/2}h^4 + \frac{4}{3}\pi\eta h^2. \quad (10)$$

with

$$B_0 = -1.960\,516\ldots, \qquad B_1 = -3.590\,668\ldots, \qquad B_2 = 4.968\,827\ldots. \quad (11)$$

The profile of the reduced half layer–layer distance $h(\eta)$ is obtained upon minimizing u with respect to h, i.e. $\partial u/\partial h = 0$, leading to

$$h^2(\eta) = -\frac{B_1\sqrt{\eta} + \frac{4}{3}\pi}{2B_2\eta^{3/2}}. \quad (12)$$

It is now a simple matter to obtain the reduced density η_c at which the monolayer–trilayer transition ($1\Delta \rightarrow 3\Delta$) takes place. The mathematical condition is thereby $h(\eta = \eta_c) = 0$ yielding

$$\sqrt{\eta_c} = -\frac{4\pi}{3B_1} \Rightarrow \eta_c = 1.360\,901\ldots, \quad (13)$$

which is in quantitative agreement with the lattice sum minimization results from the previous section, see figure 5.

By inserting the expression (13) of η_c in (12) one obtains

$$h^2(\eta) = -\frac{B_1}{2B_2}\frac{\eta - \eta_c}{\eta^2 + \eta^{3/2}\sqrt{\eta_c}}. \quad (14)$$

Noticing that the last denominator in equation (14) can be approximated (valid in the relevant limit $\eta \rightarrow \eta_c^+$) by $2\eta^2$, we obtain a square-root singularity:

$$\lim_{\eta\rightarrow\eta_c^+} h(\eta) = \sqrt{-\frac{B_1}{4B_2\eta_c^2}}(\eta - \eta_c)^{1/2} \sim (\eta - \eta_c)^{1/2}. \quad (15)$$

This theoretical prediction (14) is visualized in figure 5.

4. Multilayers

The presence of the neutralizing background allows the formation of multilayers with $m \geqslant 3$ for large enough densities η, which is forbidden in the absence of a background[5]. The physical origin of the stability of multilayers in the present system at large η is basically a balance between the mutual *unscreened* macroion–macroion repulsion and the attractive macroion–background interaction.

We shall now analyze in detail the high density regime up to $\eta \approx 130$. Beyond the bilayer regime, which is limited by 2Δ, the cascade found here upon increasing η is

$$\cdots 3\square \rightarrow 3R \rightarrow 3\Delta \rightarrow 4\square \rightarrow 4R \rightarrow 4\Delta \rightarrow 5R \rightarrow 5\Delta \rightarrow 6R\cdots, \quad (16)$$

where rhombic phases $3R$, $4R$, $5R$ and $6R$ have the stacking sequence ABA, ABAB, ABABA and ABABAB while the triangular phases 3Δ, 4Δ and 5Δ occur as ABC, ABCA and ABCAB, respectively. More structural details are given in table 1. The corresponding phase diagram is depicted in figure 6.

The primitive cells of all stable phases found in this work consist of one particle per layer. Each constitutive layer possesses the same basis shape (Δ, $\square$ or R). These layers are shifted to each other, see table 1. Note that (for $m > 3$) the layers become equidistant only in the limit $\eta \rightarrow \infty$. A remarkable finding is the absence of prism phases (at $m = 4$) that are encountered in hard-sphere systems [30, 33] and Yukawa systems at finite screening [34].

A further overview of the full phase diagram ranging from triangular monolayer to rhombic hexalayer structures is shown in figure 7 where the profile of $h(\eta)$ is also sketched. Empty circles indicate transitions of second order, while the full ones denote transitions of first order. In detail, for three and four layers, the transitions $3\square \rightarrow 3R$ and $4\square \rightarrow 4R$ occur continuously by continuously changing the angle θ between the two in-plane basis vectors, in analogy to $2\square \rightarrow 2R$

[5] There is a simple and clear electrostatic argument to explain the exclusive stability of bilayers for charges confined between (charged or uncharged) hard walls without neutralizing *volume* background. One has to note that two equally charged walls do *not* generate any electric field within the slit, and consequently do not alter the stable structure obtained at any other surface charge (including neutral walls). Hence, if one considers the special case of two walls corresponding to *two-dimensional* neutralizing backgrounds where the ground state is the 2Δ bilayer, we deduce from this that the ground-state structure is *always* a bilayer.

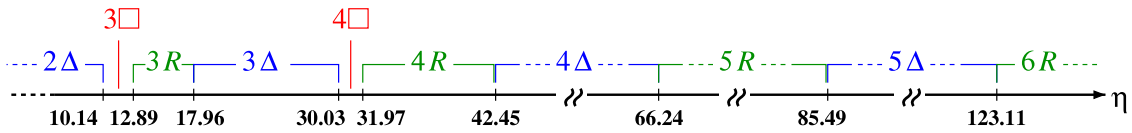

Figure 6. Stability phase diagram of crystalline multilayers in the presence of a neutralizing background. 3□, 3R, 3Δ, 4□, 4R, 4Δ, 5R, 5Δ and 6R are the stable phases in the depicted η regime.

Table 1. Structural details and schematic illustration of the stable crystalline multilayers. The layers are labeled as follows. The bottom one located at $z = -D/2$ corresponds to the first layer (labeled as $i = 1$), and the labels of the successive layers are incremented accordingly. For $m > 3$, the separation between the two first layers is characterized by δD with $1/(m-1) \leqslant \delta < 0.5$. The relative separation vector between two particles of a primitive cell belonging to two layers i and j is given by $\mathbf{d}_{ij}$. For six layers, the separation between the first and the third layers is specified by λD with $2/5 \leqslant \lambda < 0.5$. In the top views of 3Δ, 4Δ, 5Δ and 3R, 4R, 5R, 6R each basis shape (triangular or rhombic) is emphasized with white lines. The rhombic stripes of 3R, 4R, 5R and 6R are shown again in corresponding perspective views, for clarity. Particles from different layers are identified by different colors.

Phase	$\mathbf{b}/a$	$\mathbf{d}_{12}$	$\mathbf{d}_{13}$	$\mathbf{d}_{14}$	$\mathbf{d}_{15}$	$\mathbf{d}_{16}$	Top view	Side/persp. view
3□	$(0, 1)$	$\frac{\mathbf{a}+\mathbf{b}+\mathbf{c}}{2}$	$\mathbf{c}$	—	—	—	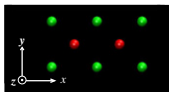	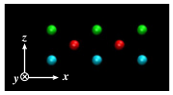
3R	$(\cos\theta, \sin\theta)$	$\frac{\mathbf{a}+\mathbf{b}+\mathbf{c}}{2}$	$\mathbf{c}$	—	—	—	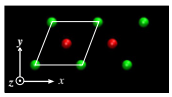	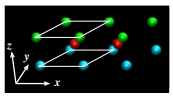
3Δ	$(1/2, \sqrt{3}/2)$	$\frac{\mathbf{a}+\mathbf{b}}{3} + \frac{\mathbf{c}}{2}$	$\frac{2(\mathbf{a}+\mathbf{b})}{3} + \mathbf{c}$	—	—	—	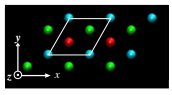	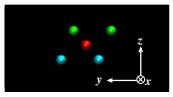
4□	$(0, 1)$	$\frac{\mathbf{a}+\mathbf{b}}{2} + \mathbf{c}\delta$	$\mathbf{c}(1-\delta)$	$\frac{\mathbf{a}+\mathbf{b}}{2} + \mathbf{c}$	—	—	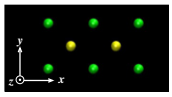	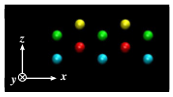
4R	$(\cos\theta, \sin\theta)$	$\frac{1}{2}(\mathbf{a}+\mathbf{b}) + \mathbf{c}\delta$	$\mathbf{c}(1-\delta)$	$\frac{1}{2}(\mathbf{a}+\mathbf{b}) + \mathbf{c}$	—	—	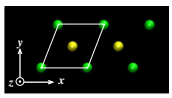	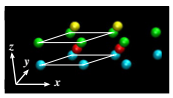
4Δ	$(1/2, \sqrt{3}/2)$	$\frac{\mathbf{a}+\mathbf{b}}{3} + \mathbf{c}\delta$	$\frac{2(\mathbf{a}+\mathbf{b})}{3} + \mathbf{c}(1-\delta)$	$\mathbf{c}$	—	—	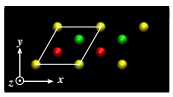	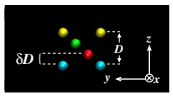
5R	$(\cos\theta, \sin\theta)$	$\frac{\mathbf{a}+\mathbf{b}}{2} + \mathbf{c}\delta$	$\frac{\mathbf{c}}{2}$	$\frac{\mathbf{a}+\mathbf{b}}{2} + \mathbf{c}(1-\delta)$	$\mathbf{c}$	—	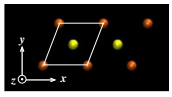	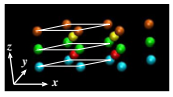
5Δ	$(1/2, \sqrt{3}/2)$	$\frac{\mathbf{a}+\mathbf{b}}{3} + \mathbf{c}\delta$	$\frac{2(\mathbf{a}+\mathbf{b})}{3} + \frac{\mathbf{c}}{2}$	$\mathbf{c}(1-\delta)$	$\frac{\mathbf{a}+\mathbf{b}}{3} + \mathbf{c}$	—	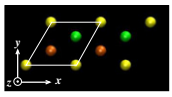	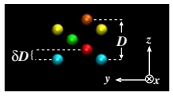
6R	$(\cos\theta, \sin\theta)$	$\frac{\mathbf{a}+\mathbf{b}}{2} + \mathbf{c}\delta$	$\mathbf{c}\lambda$	$\frac{\mathbf{a}+\mathbf{b}}{2} + \mathbf{c}(1-\lambda)$	$\mathbf{c}(1-\delta)$	$\frac{\mathbf{a}+\mathbf{b}}{2} + \mathbf{c}$	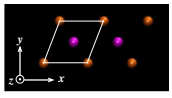	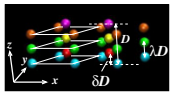

(cf figure 4), while all other transitions are discontinuous. Additionally, by the transitions 3R → 3Δ, 4R → 4Δ and 5R → 5Δ, and by the transitions changing the layer number at $\eta = 1.53$ (3Δ → 2□), $\eta = 10.14$ (2Δ → 3□), $\eta = 30.03$ (3Δ → 4□), $\eta = 66.24$ (4Δ → 5R) and $\eta = 123.11$ (5Δ → 6R) the distance between the outermost layers exhibits a certain jump Δh (indicated by thick arrows in figure 7). In fact, there is here no continuous transition present between two unequal layered phases as in the case of hard spheres[6].

Furthermore, for high densities, the concrete lattice evolves to continuous such that effects due to the concreteness are negligible. This means, electrostatically, that each layer of an m-layered structure is completely compensated by a certain part of the background as much as $1/m$ of the whole.

In this paper we have dealt with a system consisting of particles (*macroions*) interacting via the unscreened Coulomb potential and of particles of opposite charge (*counterions*), which are homogeneously smeared out over a hard slit of width L, compensating the charge of the macroions. To determine the stability diagram of crystalline phases, we have performed lattice sum calculations of a set of candidates. As possible candidates we have taken into account phases with up to six layers ($m = 1, \ldots, 6$) whose primitive cell contains up to eight particles ($n = 1, \ldots, 8$). Additionally, we considered the

[6] In the case of bilayered hard spheres, one can achieve a continuous layer increase from 2Δ to four layered hcp-like and hcp(100) phase [31, 32, 34].

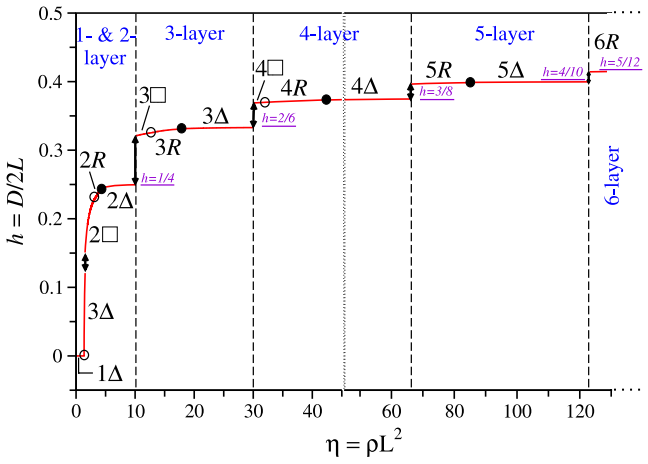

Figure 7. Order parameter h of all stable crystalline phases. Empty circles denote a continuous transition, whereas the full circles mark a discontinuous one. The transitions between phases with a different number of layers ($m \to m+1$) correspond to a first-order transition for ($m \geqslant 2$). The underlined values of $h = \frac{m-1}{2m}$ correspond to the limit $\eta \to \infty$ at constant m. The vertical dotted line indicates a scale change in the η axis.

buckling phases from [50], too. We have analyzed a regime up to $\eta \approx 130$ in our investigations. For small densities, we could trace the existence of the triangular monolayer 1Δ. Crossing a certain critical density η_c the system buckles and evolves to a trilayered structure. This transition density is also calculated analytically by applying a Taylor expansion to the lattice sum for small separations. Furthermore the evolving of the layer separation from monolayer to trilayer could be characterized as $h(\eta) \sim (\eta - \eta_c)^{1/2}$, qualitatively. Tuning the density upwards, we have noticed different stable bilayered structures, the same as Wigner crystals. Beyond the bilayers, we could also find stable three, four, five and six layers in square, rhombic and triangular bases. The final stability sequence for $m > 4$ is therefore: $mR \to m\Delta \to (m+1)R$ with a remarkable vanishing of square-based phases, where the sequence for $m = 3$ and 4 is $m\square \to mR \to m\Delta \to (m+1)\square$. While the stability domain of evenly layered phases gets larger with increasing m, the stability domain of square phases ($\square$) decreases for $m > 2$ and disappears finally for $m > 5$. On the other hand, the stability domain of rhombic (R) and triangular (Δ) phases increases both with growing $m > 2$.

Apart from that, the transitions involved here are all of second order except $mR \to m\Delta$ and $m\Delta \to (m+1)\square$. The latter takes place discontinuously due to the order parameter θ and particle positions (as in the case of $nR \to n\Delta$) as well as with respect to h (cf figure 7).

5. Conclusions

To summarize: for slit-confined ions in a smeared background, we have determined the ground-state crystalline lattice as a function of the ion density up to the six-layer regime. A complex cascade with buckled, squared and triangular bi, tri, tetra, penta and hexalayers was found. The results are verifiable in systems with classical ions in a background including charged colloids, dusty plasmas and classical ions in a trap. One important conclusion is that the details of multilayered structures depend crucially on the particle–background interaction. More future work is needed to include wall charges, wall–particle attractions and effects of finite temperature [54]. A detailed understanding of the stable crystalline structure as originating from the wall properties is desirable to construct filter devices [45] or optical bandgap crystals [55].

Acknowledgments

We thank T Palberg and S Apolinario for helpful discussions. This work was supported by the DFG via the SFB TR6 (project D1).

Appendix

The total interaction energy per unit cell of a crystalline unscreened Coulomb system can be written as

$$U_C = U_C^s + U_C^c, \tag{A.1}$$

where the unit cell consists of n particles of charge q located at $\mathbf{r}_i$. The self-energy U_C^s in equation (A.1) stems from the interaction between a particle of the unit cell and its own periodically repeated images. The term U_C^s in equation (A.1) is due to the interaction between a particle of the unit cell and all other remaining $n-1$ particles of the cell including their own images. The convergence involved in these sums is guaranteed by the inclusion of a *surface* neutralizing background for each layer. Following the route of Bródka and Grzybowski (see equations (16*a*), (16*b*) and (17) of [48]), U_C^s and U_C^c are given below. Therefore U_C^s is

$$U_C^s = \frac{1}{|a_x|} n \frac{q^2}{\epsilon} \left\{ 4 \left(\sum_{m,k=1}^{\infty} \cos\left(2\pi k \frac{b_x}{a_x} m\right) K_0\left(2\pi k \left|\frac{b_y}{a_x}\right| m\right)\right) + \gamma_e - \ln\left(4\pi \left|\frac{a_x}{b_y}\right|\right)\right\}, \tag{A.2}$$

with $\gamma_e = 0.577\,215\,665$ denoting the Euler–Mascheroni constant, $K_0(x)$ the modified Bessel function of the second kind [56] and a_x, b_x and b_y the corresponding x and y components of the lattice vectors $\mathbf{a}$ and $\mathbf{b}$. Using the components $x_{ij} = x_i - x_j$, $y_{ij} = y_i - y_j$ and $z_{ij} = z_i - z_j$ of the relative separation vector $\mathbf{r}_{ij}$ between cell particles i and j, U_C^c can be written as

$$U_C^c = \frac{1}{|a_x|} \sum_{i=1}^{n} \sum_{\substack{j=1 \\ j>i}}^{n} \frac{q^2}{\epsilon} \times \left\{ 4 \sum_{m,k=1}^{\infty} \left[\cos\left(2\pi k \frac{x_{ij} + b_x m}{a_x}\right) \times K_0\left(2\pi k \left[\frac{(y_{ij} + b_y m)^2 + z_{ij}^2}{a_x^2}\right]^{1/2}\right) + \cos\left(2\pi k \frac{x_{ij} - b_x m}{a_x}\right)\right.\right.$$

$$\times K_0\left(2\pi k\left[\frac{(y_{ij}-b_y m)^2+z_{ij}^2}{a_x^2}\right]^{1/2}\right)\Bigg] + 4\sum_{k=1}^{\infty}\cos\left(2\pi k\frac{x_{ij}}{a_x}\right)K_0\left(2\pi k\left[\frac{y_{ij}^2+z_{ij}^2}{a_x^2}\right]^{1/2}\right) - \ln\left[\cosh\left(2\pi\left|\frac{z_{ij}}{b_y}\right|\right)-\cos\left(2\pi\frac{y_{ij}}{b_y}\right)\right]-\ln 2\Bigg\} \quad (A.3)$$

for $(y_{ij}, z_{ij}) \neq (0,0)$ and

$$U_{\mathrm{C}}^{\mathrm{c}} = \frac{1}{|a_x|}\sum_{i=1}^{n}\sum_{\substack{j=1\\ j>i}}^{n}\frac{q^2}{\epsilon} \times\Bigg\{4\sum_{m=1}^{\infty}\sum_{k=1}^{\infty}\Bigg[\cos\left(2\pi k\frac{x_{ij}+b_x m}{a_x}\right)K_0\left(2\pi k\left|\frac{b_y m}{a_x}\right|\right) + \cos\left(2\pi k\frac{x_{ij}-b_x m}{a_x}\right)K_0\left(2\pi k\left|\frac{b_y m}{a_x}\right|\right)\Bigg] - 2\psi\left(\left|\frac{x_{ij}}{ax}\right|\right)-\pi\cot\left(\pi\left|\frac{x_{ij}}{a_x}\right|\right)-2\ln\left(4\pi\left|\frac{a_x}{b_y}\right|\right)\Bigg\} \quad (A.4)$$

for $(y_{ij}, z_{ij}) = (0,0)$, where $\psi(x)$ is the digamma function [56].

Being interested in the transition from mono to trilayers, we take as input the structure characteristics of the triangular phase 1Δ into the lattice sums (A.2)–(A.4): $\theta = \pi/3$, $b_x/a_x = 0.5$, $b_y/a_x = \sqrt{3}/2$, $\gamma = 1$, $x_{12}/a_x = 0.5 = x_{23}/a_x$, $= y_{12}/b_y = 1/3 = y_{23}/b_y$, $x_{13}/a_x = 1$, $y_{13}/b_y = 2/3$, $\rho = N/A = \frac{3}{a_x b_y} = \frac{2\sqrt{3}}{{a_x}^2}$ and therefore ${a_x}^2 = \frac{2\sqrt{3}}{\rho} = \frac{2\sqrt{3}L^2}{\eta}$. Here we consider for 1Δ a multicell ($n = 3$) consisting of three primitive cells, containing each 1 particle. Thus, for a given η, the energy function U_{C} depends now only on $z_{12} = hL = z_{23}$. Taking this feature into account, the self-energy and the cross-energy finally are

$$U_{\mathrm{C}}^{\mathrm{s}} = \frac{1}{|a_x|}3\frac{q^2}{\epsilon}\Bigg\{4\sum_{m,k=1}^{\infty}\cos(\pi km)\,K_0(\pi km\sqrt{3}) + \gamma_{\mathrm{e}} - \ln\left(\frac{8\pi}{\sqrt{3}}\right)\Bigg\} \quad (A.5)$$

and

$$U_{\mathrm{C}}^{\mathrm{c}}(h) = \frac{1}{|a_x|}\sum_{i=1}^{3}\sum_{\substack{j=1\\ j>i}}^{3}\frac{q^2}{\epsilon} \times\Bigg\{4\sum_{m,k=1}^{\infty}\Bigg[\cos\left(2\pi k\frac{x_{ij}+b_x m}{a_x}\right) \times K_0\left(2\pi k\left[\lambda_{ij}^{+2}+\beta_{ij}^2 h^2\right]^{1/2}\right) + \cos\left(2\pi k\frac{x_{ij}-b_x m}{a_x}\right)K_0\left(2\pi k\left[\lambda_{ij}^{-2}+\beta_{ij}^2 h^2\right]^{1/2}\right)\Bigg] + 4\sum_{k=1}^{\infty}\cos\left(2\pi k\frac{x_{ij}}{a_x}\right)K_0\left(2\pi k\left[\frac{y_{ij}^2}{a_x^2}+\beta_{ij}^2 h^2\right]^{1/2}\right) - \ln\left[\cosh(2\pi|\phi_{ij}|h)-\cos\left(2\pi\frac{y_{ij}}{b_y}\right)\right]-\ln 2\Bigg\}, \quad (A.6)$$

where $\lambda_{12}^{\pm} = \sqrt{(y_{12}\pm b_y m)^2/a_x^2} = \sqrt{3/4}(1/3\pm m) = \lambda_{23}^{\pm}$, $\lambda_{13}^{\pm} = \sqrt{(y_{13}\pm b_y m)^2/a_x^2} = \sqrt{3/4}(2/3\pm m)$, $\beta_{12} = L/a_x = \beta_{23}$, $\beta_{13} = 2L/a_x$, $\phi_{12} = \sqrt{2\eta/3\sqrt{3}} = \phi_{23}$ and $\phi_{13} = 2\sqrt{2\eta/3\sqrt{3}}$. Before expanding the energy function at $h = 0$, we first define

$$f(h)^{\pm} = K_0\left(2\pi k\left[\lambda^{\pm 2}+\beta^2 h^2\right]^{1/2}\right), \quad (A.7)$$

where the first four derivatives of $f(h)$ at $h = 0$ are given as follows:

$$f(0)^{\pm} = K_0\left(2\pi k\lambda^{\pm}\right), \quad (A.8)$$

$$f'(0)^{\pm} = 0, \quad (A.9)$$

$$f''(0)^{\pm} = -K_1\left(2\pi k\lambda^{\pm}\right)\frac{2\pi k\beta^2}{\lambda^{\pm}}, \quad (A.10)$$

$$f'''(0)^{\pm} = 0, \quad (A.11)$$

$$f''''(0)^{\pm} = \left[K_0\left(2\pi k\lambda^{\pm}\right)2\pi k\lambda^{\pm} + 2K_1\left(2\pi k\lambda^{\pm}\right)\right]\frac{3\beta^4 2\pi k}{\lambda^{\pm 3}}. \quad (A.12)$$

Here, $K_1(x)$ is a modified Bessel function of the second kind [56], too. Using a Taylor series and (A.8)–(A.12), we now expand $U_{\mathrm{C}}(h)$ from (A.1) at $h = 0$ and achieve the final form of the energy:

$$\frac{\epsilon u(h)}{q^2\sqrt{\rho}} = \underbrace{-1.960\,516 - 3.590\,668\eta h^2 + 4.968\,827\eta^2 h^4}_{\frac{U_{\mathrm{C}}(h)\epsilon}{3q^2\sqrt{\rho}}} + \tfrac{4}{3}\pi h^2\sqrt{\eta}. \quad (A.13)$$

The last term stems from (5), due to interactions with the background, respectively. The coefficient $-1.960\,516$ corresponds to the static energy per particle of the triangular lattice, which was already calculated in [57].

References

[1] Levin Y 2002 *Rep. Prog. Phys.* **65** 1577
[2] Messina R 2009 *J. Phys.: Condens. Matter* **21** 113102
[3] Löwen H, Madden P A and Hansen J P 1992 *Phys. Rev. Lett.* **68** 1081
[4] Löwen H, Hansen J P and Madden P A 1993 *J. Chem. Phys.* **98** 3275
[5] Löwen H 1994 *J. Chem. Phys.* **100** 6738
[6] Hansen J-P and Löwen H 2000 *Ann. Rev. Phys. Chem.* **51** 209
[7] Levin Y and Arenzon J J 2003 *J. Phys. A: Math. Gen.* **36** 5857
[8] Orkoulas G, Panagiotopoulos A Z and Fisher M E 2000 *Phys. Rev.* E **61** 5930
[9] Levin Y 2002 *J. Phys.: Condens. Matter* **14** 2303
[10] Allahyarov E, D'Amico I and Löwen H 1998 *Phys. Rev. Lett.* **81** 1334
[11] Messina R, Holm C and Kremer K 2000 *Phys. Rev. Lett.* **85** 872
[12] Allahyarov E, Gompper G and Löwen H 2004 *Phys. Rev.* E **69** 041904
[13] Allahyarov E *et al* 2007 *Europhys. Lett.* **78** 38002
[14] Leunissen M E *et al* 2005 *Nature* **437** 235
[15] Hynninen A P *et al* 2006 *Phys. Rev. Lett.* **96** 138308
[16] Murray C A and Grier D G 1996 *Annu. Rev. Phys. Chem.* **47** 421
[17] Klumov B A and Morfill G E 2008 *J. Exp. Theor. Phys.* **107** 908

[18] Fontecha A B and Schöpe H J 2008 *Phys. Rev.* E **77** 061401
[19] Cohen I, Mason T G and Weitz D A 2004 *Phys. Rev. Lett.* **93** 046001
[20] Klapp S H L, Zeng Y, Qu D and von Klitzing R 2008 *Phys. Rev. Lett.* **100** 118303
[21] Lobaskin V, Brunner M, Bechinger C and von Grünberg H H 2003 *J. Phys.: Condens. Matter* **15** 6693
[22] Löwen H and Kramposthuber G 1993 *Europhys. Lett.* **23** 673
[23] Löwen H and Allahyarov E 1998 *J. Phys.: Condens. Matter* **10** 4147
[24] Allahyarov E, D'Amico I and Löwen H 1999 *Phys. Rev.* E **90** 3199
[25] Russ C, von Grünberg H H, Dijkstra M and van Roij R 2002 *Phys. Rev.* E **66** 011402
[26] Russ C, Brunner M, Bechinger C and von Grünberg H H 2005 *Europhys. Lett.* **69** 468
[27] Dobnikar J, Castaneda-Priego R, von Grünberg H H and Trizac E 2006 *New J. Phys.* **8** 277
[28] Messina R and Löwen H 2003 *Phys. Rev. Lett.* **91** 146101
[29] Fontecha A B *et al* 2005 *J. Phys.: Condens. Matter* **17** S2779
[30] Neser S, Bechinger C, Leiderer P and Palberg T 1997 *Phys. Rev. Lett.* **79** 2348
[31] Ramiro-Manzano F, Bonet E, Rodriguez I and Meseguer F 2007 *Phys. Rev.* E **76** 050401(R)
[32] Fontecha A B, Palberg T and Schöpe H J 2007 *Phys. Rev.* E **76** 050402(R)
[33] Fortini A and Dijkstra M 2006 *J. Phys.: Condens. Matter* **18** 371
[34] Oğuz E C, Messina R and Löwen H 2009 *Europhys. Lett.* **86** 28002
[35] Grandner S and Klapp S H L 2008 *J. Chem. Phys.* **129** 244703
[36] Goldoni G and Peeters F M 1995 *Phys. Rev.* B **53** 4591
[37] Apolinario S W S, Partoens B and Peeters F M 2007 *New J. Phys.* **9** 283
[38] Cornelissens Y G, Partoens B and Peeters F M 2000 *Physica* E **8** 314
[39] Drocco J A, Reichhardt C J O, Reichhardt C and Janko B 2003 *Phys. Rev.* E **68** 060401
[40] Totsuji H, Kishimoto T and Totsuji C 1997 *Phys. Rev. Lett.* **78** 3113
[41] Rahman A and Schiffer J P 1986 *Phys. Rev. Lett.* **57** 1133
[42] Totsuji H and Barrat J-L 1988 *Phys. Rev. Lett.* **60** 2484
[43] Schiffer J P 1988 *Phys. Rev. Lett.* **61** 1843
[44] Ren C I and Ma Y Q 2006 *J. Am. Chem. Soc.* **128** 2733
[45] Yan F and Goedel W A 2004 *Chem. Mater.* **16** 1622
[46] Messina R 2002 *J. Chem. Phys.* **117** 11062
[47] Lekner J 1991 *Physica* A **176** 485
[48] Bródka A and Grzybowski A 2002 *Mol. Phys.* **100** 1017
[49] Mazars M 2008 *Europhys. Lett.* **84** 55002
[50] Chou T and Nelson D R 1993 *Phys. Rev.* E **48** 4611
[51] Pansu B, Pieranski P and Pieranski P 1984 *J. Physique* **45** 331
[52] Neser S, Leiderer P and Palberg T 1997 *Prog. Colloid Polym. Sci.* **102** 194
[53] Schmidt M and Löwen H 1996 *Phys. Rev. Lett.* **76** 4552
[54] Donko Z, Kalman G J and Hartmann P 2008 *J. Phys.: Condens. Matter* **20** 413101
[55] Manoharan V N, Elsesser T and Pine D J 2003 *Science* **301** 483
[56] Abramowitz M and Stegun I A 1965 *Handbook of Mathematical Functions* (New York: Dover)
[57] Maradudin A A and Bonsall L 1977 *Phys. Rev.* B **15** 1959